International Journal of Innovative Research in Computer Science and Technology (IJIRCST)
ISSN (Online): 2347-5552, Volume-14, Issue-6, Nov-Dec 2026
DOI: https://doi.org/10.55524/ijircst.2026.14.6.5
Article ID IRP-1805, Pages 38-47
www.ijircst.org

Experimental Evaluation of Hall Sensor Placement for Gap Sensing in a Magnetic Levitation Setup

Okan Uyar

Assistant Professor, Department of Mechatronics Engineering, Faculty of Technology, Selçuk University, Konya, Türkiye

Correspondence should be addressed to Okan Uyar; okanuyar@selcuk.edu.tr

Received: 20 Oct 2026; **Revised:** 4 Nov 2026**:** **Accepted:** 16 Nov 2026; **Published Online:** 18 Nov 2026

Copyright © 2026 Okan Uyar. This is an open-access article distributed under the Creative Commons Attribution 4.0 International License (CC BY 4.0), which permits unrestricted use, distribution, and reproduction in any medium, provided the original work is properly cited.

ABSTRACT- Hall-effect sensors can measure the air gap in magnetic levitation inexpensively, but the electromagnet field is superimposed on that of the levitated magnet. This study compares two sensor locations on a pot-type electromagnet levitating an NdFeB magnet: a linear Hall sensor on the pole face (S1) and a second sensor close to the back face (S2). The outputs were recorded at 11 gaps between 11 and 30 mm, for coil currents between 0 and 0.25 A and lateral positions of up to ±4 mm (214 readings). A separate lift-off test placed the estimated levitation window between 14.4 and 26.6 mm. S1 was about 21 times more gap-sensitive than S2 (20.5 versus 0.95 mV/mm at 21 mm), but its coil contribution at the rated current equalled an apparent gap change of about 30 mm. For S1 this contribution was nearly linear, gap-independent and almost unchanged by the magnet. A current coefficient identified on the increasing branch of a sweep left an equivalent current residual of 0.26 mm on the decreasing branch of the same sweep (window median; 0.96 mm at 21 mm); a single coefficient from other gaps or from the coil-only test left about 1.8 mm on the same readings. The dual-sensor difference performed worse (6.1 mm) because the coil-cancelling ratio exceeded the magnet sensitivity ratio. For the accepted lateral profiles, ±2 mm changed the S1 reading by the equivalent of 0.3–1.0 mm. A centred pole-face sensor with a current coefficient identified near the operating gap is recommended.

KEYWORDS- Current Compensation, Gap Sensing, Hall-Effect Sensor, Magnetic Levitation, Sensor Placement

I. INTRODUCTION

Magnetic levitation (maglev) keeps an object suspended without mechanical contact and is used in transport, frictionless bearings, precision positioning and, at laboratory scale, as a standard platform for teaching and testing nonlinear control [1]–[5]. A single-electromagnet levitator is open-loop unstable, so its controller depends on a continuous measurement of the air gap. Optical barriers and photo-sensor arrays are common in educational rigs [1], [2], laser and eddy-current sensors offer high accuracy at a higher cost, and Hall-effect sensors are attractive when a permanent magnet is levitated, because the magnet itself provides the field that encodes its position [6]–[8].

The difficulty with Hall sensing is that the electromagnet also produces a field at the sensor. When the control current changes, the sensor cannot distinguish a change of coil field from a movement of the magnet. Two remedies are used in practice. The first measures the coil current and subtracts its contribution from a single sensor [6], [9]. The second places two sensors at the two ends of the electromagnet and subtracts their outputs, on the assumption that the coil field is the same at both ends, whereas the magnet field is much weaker at the far end [8]. More elaborate arrangements use several symmetric sensors to reject tilt and lateral offset [6], [7], or sensor arrays with polynomial or learned position estimators [10], [11]. Near strong magnets the sensor may also leave its linear range, which constrains its location [12].

Although both remedies are widely used, their performance is rarely compared on the same hardware, and the influence of the sensor location and of the electromagnet construction is seldom quantified. Many low-cost levitators [7], [13] use pot-type holding electromagnets with a closed steel case, for which the symmetry assumed by the dual-sensor scheme is doubtful. This paper reports a static experimental evaluation of two Hall-sensor locations on such an electromagnet. Its contributions are: (i) a calibrated comparison of a pole-face sensor and a sensor near the back face over the full levitation window; (ii) a quantification of the coil interference and a test of field superposition with the magnet in place; (iii) a measurement of the lateral cross-sensitivity, interpreted with an analytical magnet model; and (iv) a comparison of four measurement architectures in terms of equivalent gap error on readings not used to identify their coefficients, with an uncertainty budget for the recommended one.

Section II describes the measurement principle and the architectures, Section III the set-up and procedure, Section IV the results, Section V their implications for sensor placement, and Section VI concludes the paper.

II. MEASUREMENT PRINCIPLE

A. Field Superposition at the Sensors

A linear Hall sensor gives an output voltage proportional to the flux density normal to its face. With the magnet at gap z and lateral offset x and a coil current I, the output of sensor j can be written as

$$V_j = V_{0,j} - G_j B_m(z,x) + a_j I, \qquad j = 1,2 \tag{1}$$

where $V_{0,j}$ is the zero-field output, G_j an effective gain that includes the sensor sensitivity and the flux concentration by the steel, B_m the field of the magnet and a_j the coil

coefficient (output change per ampere). Equation (1) holds if the coil and magnet contributions superpose, which is tested in Section IV-B. In the set-up used here the attraction polarity makes both contributions lower the output of S1.

B. Magnet Field Model

On the axis of an axially magnetised cylinder of radius R, thickness L and remanence B_r, the flux density at distance d from its face is [14], [15]

$$B_z(r=0,d)=\frac{B_r}{2}\left[\frac{L+d}{\sqrt{R^2+(L+d)^2}}-\frac{d}{\sqrt{R^2+d^2}}\right] \quad (2)$$

The off-axis component used for the lateral analysis was computed from the equivalent surface-current model with complete elliptic integrals [14]. The calibration curve of each sensor is

$$V_1(z)=V_0-G\,B_z(0,\,z+\delta) \quad (3)$$

where δ is an effective offset between the face of the electromagnet and the sensing element. V_0, G and δ were fitted to the calibration readings by least squares. The local sensitivity is

$$S_j(z)=\frac{\mathrm{d}V_j}{\mathrm{d}z} \quad (4)$$

C. Measurement Architectures

Four ways of obtaining the gap from the sensor outputs were compared. M1 uses S1 alone and M2 uses S2 alone. M3 subtracts the coil contribution from S1 using the measured current, and M4 subtracts a scaled S2 output from S1 so that the coil contributions cancel:

$$V_3=V_1-aI,\qquad V_4=V_1-kV_2,\quad k=a_1/a_2 \quad (5)$$

The coefficient a or k was obtained in three ways: identified with the magnet in place at the same gap from the increasing branch of the current sweep (same gap); as the mean of the coefficients identified at the other ten gaps (other gaps, M3 only); or from the test with the magnet removed (coil only). All variants were evaluated on the same readings, the decreasing branch of each sweep. The gap sensitivity of the dual-sensor signal is

$$S_4=S_1-k\,S_2 \quad (6)$$

Equation (6) shows the condition for a useful difference signal: the ratio of the magnet sensitivities S_1/S_2 must be much larger than the ratio of the coil coefficients k. Otherwise the difference loses, or even inverts, its gap information.

D. Equivalent Gap Error

Every voltage error ΔV was converted to an equivalent gap error with the local sensitivity,

$$e=\frac{\Delta V}{|S|} \quad (7)$$

so that the noise, the residual coil contribution, the lateral offset and the drift of the architectures can be compared on one scale.

III. EXPERIMENTAL SETUP AND PROCEDURE

A. Test Rig

The rig is shown in Figure 1. A 12 V pot-type holding electromagnet (Ø50 mm × 25 mm, steel case with a centre pole and an outer ring, coil resistance about 46 Ω) was mounted face up on an X stage. A 3D-printed support raised the electromagnet above the linear encoder of the stage, to keep the encoder away from the magnetic field, and also carried the holder of the lower sensor; the effect of this separation on the encoder was not quantified. An N35 NdFeB cylinder (15 mm × 5 mm) was held above it on the arm of a ball-screw Z carriage, with the attraction polarity, so that the gap z between the magnet face and the pole face could be set without levitation. Two SS49E linear Hall sensors [16] were used: S1 on the pole face, facing the magnet, and S2 in a 3D-printed holder close to the bottom (back) face of the case. Both were read by an ADS1115 16-bit converter [17] (±6.144 V range, 0.1875 mV per code, 128 samples/s) connected to an Arduino Uno; the two channels (A0 = S1, A1 = S2) were converted sequentially, and each reading in the data set is the mean of 200 sample pairs logged by a Python interface. The lateral position was read from an ALS4 incremental linear encoder (5 µm per count) on the X stage; its zero (x = 0) was set where the magnet holder was aligned with the axis of the electromagnet, using a scribed reference line. The Hall sensors were placed close to the centres of the two faces without a millimetric reference. The gap was set with a caliper. The coil was supplied from an OWON ODP3063 laboratory supply operated in current limit, and the current values are the readings of the supply display; the current was not measured independently. The components are summarised in Table 1.

Table 1: Components and measurement conditions

Item	Specification
Electromagnet	12 V DC pot-type holding magnet, Ø50 mm × 25 mm, steel case, R ≈ 46 Ω, rated current 0.25 A
Levitated magnet	NdFeB N35, Ø15 mm × 5 mm, axial magnetisation, B_r ≈ 1.19 T
Hall sensors	2 × SS49E; S1 on pole face, S2 in 3D-printed support near back face
Valid reading	1.0–4.0 V (acquisition-software threshold)
Converter	ADS1115, 16 bit, ±6.144 V, 0.1875 mV/LSB, 128 SPS
Reading	Mean of 200 sample pairs, channels read sequentially (Arduino Uno, Python logger)
Gap z	11, 13, 15, 17, 19, 20, 21, 23, 25, 27, 30 mm (caliper)
Lateral offset x	−4, −2, 0, 2, 4 mm (ALS4 encoder, 5 µm/count)
Coil current I	0, 0.08, 0.17, 0.25 A (OWON ODP3063, current limit; display reading)
Readings	214 (coil only 7, main 165, noise 20, repeats 22)

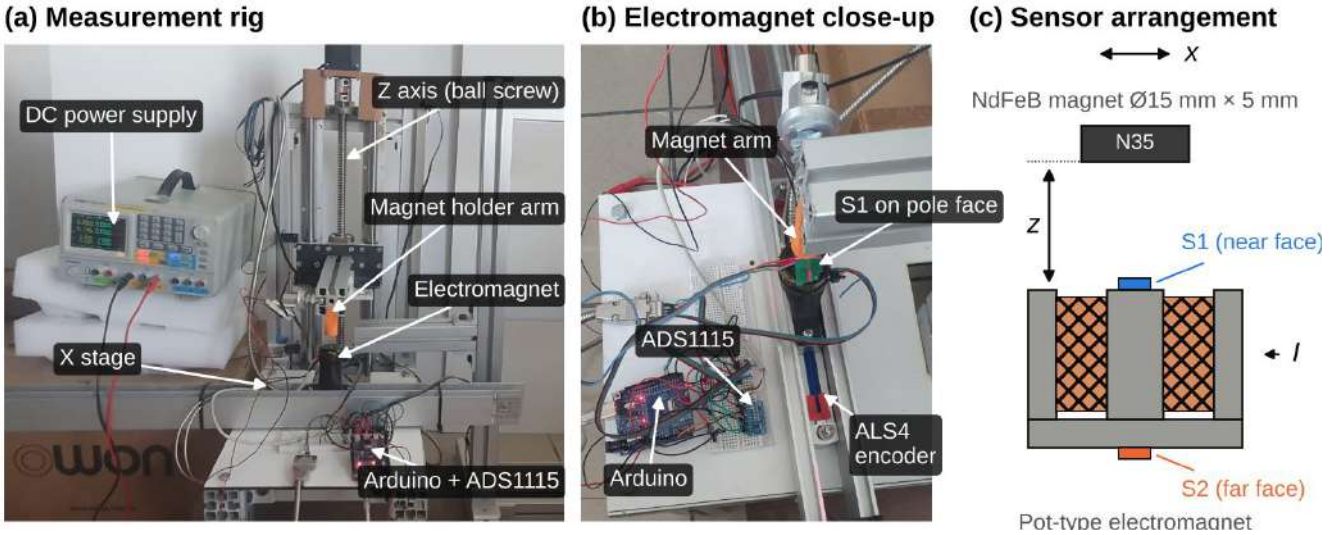


Figure 1: Experimental set-up: (a) measurement rig with the Z carriage holding the magnet above the electromagnet on the X stage; (b) close-up of the electromagnet with S1 on the pole face, the linear encoder and the electronics; (c) sensor arrangement and coordinates.

B. Jump Test and Levitation Window

Before the static measurements the levitation range was estimated with a separate lift-off (jump) test. For this test the electromagnet was mounted face down with a 1 mm plastic sheet (thickness measured with a caliper) on its pole face, and the magnet rested on a support below it. With the coil current fixed, the gap was reduced in small steps until the magnet jumped up to the sheet; at that gap the upward attraction just exceeds the weight of the magnet, so the jump gap approximates the gap at which the static attraction equals the weight. The caliper reading was taken from the surface of the sheet to the far face of the magnet, so the gap to the pole face is the reading minus the 5 mm magnet thickness plus the 1 mm sheet. Three repetitions were made at 0, 0.25 and 0.5 A; the 0.5 A test, at twice the rated current, was kept short to avoid heating the coil. The jump gaps were 14.4 ± 0.2, 26.6 ± 0.3 and 33.3 ± 0.3 mm, so the estimated levitation window at the rated current extends from 14.4 to 26.6 mm. A quadratic fit through the three points gives the holding current along the window; the gap held by half the rated current, 21.2 mm, was taken as the operating gap (21 mm). In the static sensor measurements, the electromagnet was mounted face up (Figure 1) and the magnet was held by the arm, so the orientation matters only for the lift-off test.

C. Measurement Plan

At each of the 11 gaps the current was stepped through 0, 0.08, 0.17, 0.25, 0.17, 0.08 and 0 A at $x = 0$, and readings were taken at $x = -4$, -2, 2 and 4 mm at 0 and 0.25 A (15 readings per gap). In addition, seven readings followed the same current sequence with the magnet removed (coil only); ten consecutive readings at 0 A and ten at 0.25 A were taken at the operating gap without touching the rig (noise group); and two further sweeps over all gaps were made at $x = 0$, $I = 0$ (repeat sweeps). The data set thus contains 214 readings.

D. Data Processing

The acquisition software flagged readings outside 1.0–4.0 V, and these were excluded from all fits. The threshold is a software limit set within the lower end of the SS49E output span (1.05 V minimum, 0.95 V typical [16]); it is not a measured saturation point, and the readings below it is reported but not interpreted as saturated. The calibration model (3) was fitted to the three zero-current readings at each gap (main sweep and two repeat sweeps, 33 readings per sensor). The coil coefficient at each gap was obtained by least squares from the increasing branch of the current sweep (0.08, 0.17 and 0.25 A) through the zero-current reading. The decreasing branch (0.17, 0.08 and 0 A) was kept for validation: the compensation residuals of all coefficient variants are evaluated on these readings, which were not used to identify the same-gap coefficient.

A lateral profile was used for the model comparison when (i) at least one pair of readings at 0 and 0.25 A at $x \neq 0$ was available and its coil coefficient agreed within 10% with that at $x = 0$, which must hold because S1 moves with the electromagnet, and (ii) the fitted magnet axis had a standard error below 1 mm. Seven of the eleven profiles met both conditions. The profiles at 15 and 17 mm deviated by 61% and 29% in coil coefficient, the profile at 30 mm was too flat to locate the axis, and at 11 mm no pair was usable because all 0.25 A readings were below 1.0 V. Uncertainties were combined following the GUM [18].

IV. RESULTS

A. Static Calibration and Sensitivity

Figure 2 shows the zero-current outputs of both sensors. The model (3) described S1 with $R^2 = 0.997$ and a residual standard deviation of 10.8 mV, and S2 with $R^2 = 0.909$ and 2.8 mV (Table 2). The S1 sensitivity fell from 114 mV/mm at 11 mm to 6.6 mV/mm at 30 mm and was 59.4 and 9.8 mV/mm at the lower and upper edges of the levitation window. S2 was 21–22 times less sensitive at every gap (0.95 mV/mm at 21 mm), as expected for a sensor farther from the magnet and behind the steel case. With the record-to-record noise of S1 (0.56 mV, Section IV-E) the noise-limited resolution of S1 at the operating gap is 0.027 mm, and the converter resolution corresponds to 0.009 mm.

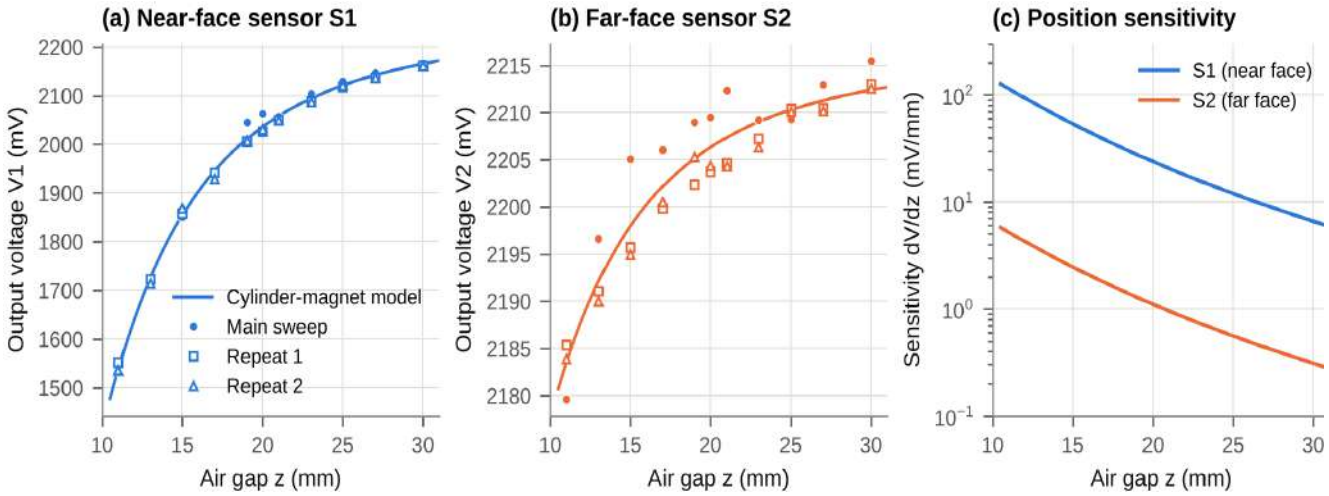


Figure 2: Static calibration at $x = 0$ and $I = 0$: (a) S1 and (b) S2 output versus gap with the fitted cylinder-magnet model; (c) gap sensitivity of both sensors. Three readings per gap (main sweep and two repeat sweeps).

Table 2: Calibration parameters and gap sensitivity

Quantity	S1 (near face)	S2 (far face)
V_0 (mV)	2243.7 ± 9.3	2216.1 ± 2.5
G (mV/mT)	19.7 ± 2.9	0.96 ± 0.80
δ (mm)	1.65 ± 0.85	2.0 ± 4.9
Residual SD (mV) / R^2	10.8 / 0.997	2.8 / 0.909
Sensitivity at 15 mm (mV/mm)	53.6	2.46
Sensitivity at 21 mm (mV/mm)	20.5	0.954
Sensitivity at 25 mm (mV/mm)	11.9	0.557
Noise-limited resolution at 21 mm (mm)	0.027	0.63

Parameter values are given with one standard error; 33 readings per sensor.

B. Coil Interference and Superposition

With the magnet removed, the coil changed the outputs linearly by $a_1 = -3283 \pm 15$ mV/A ($R^2 = 0.9999$) and $a_2 = -62 \pm 15$ mV/A (Table 3, Figure 3). At the rated current the S1 output therefore moved by 823 mV, which equals an apparent gap change of about 40 mm at the operating gap. With the magnet present the effect is equally large: at 30 mm the S1 output fell by 865 mV between 0 and 0.25 A, more than the 633-mV change produced by moving the magnet from 30 to 11 mm at zero current. The coil-only change at S2 was about 2% of that at S1; the S2 coil-only fit is less certain ($R^2 = 0.76$) because its 18-mV change is comparable to the reading scatter.

With the magnet present (Figure 3a, b) the coil contribution at every gap followed the coil-only line. The coefficient a_1 averaged −3271 mV/A, only 0.4% from the coil-only value, varied between −2934 and −3694 mV/A (coefficient of variation 7.6%) and showed no systematic trend with gap (correlation 0.29, Fig. 3c). Within the measured conditions, a linear current correction of S1 is therefore approximately valid, which supports the feed-forward compensation M3; the gap-to-gap scatter of 7.6% sets the limit of a fixed coefficient. S2 behaved differently: its coefficient changed from −62 mV/A without to $a_2 = -98 \pm 6$ mV/A with the magnet, so the two contributions do not simply add at S2, and the ratio $k = a_1/a_2$ ranged from 27 to 41, against 53 from the coil-only test. The coil step in the noise group gave consistent values (−3492 and −95 mV/A). The difference between the decreasing and increasing branches was at most 3.3 mV for gaps of 13 mm and above.

Table 3: Coil coefficients without and with the magnet

Quantity	S1	S2
Coil only: a (mV/A)	−3283 ± 15	−62 ± 15
Coil only: R^2	0.9999	0.765
Coil only: change at 0.25 A (mV)	−822.8	−18.3
Magnet present: mean a (mV/A)	−3271	−98.0
Magnet present: SD / range (mV/A)	249 / −3694 to −2934	5.8 / −109 to −91
Noise group: a (mV/A)	−3492	−95.1
Ratio $k = a_1/a_2$	27–41 (magnet present); 53 (coil only)	

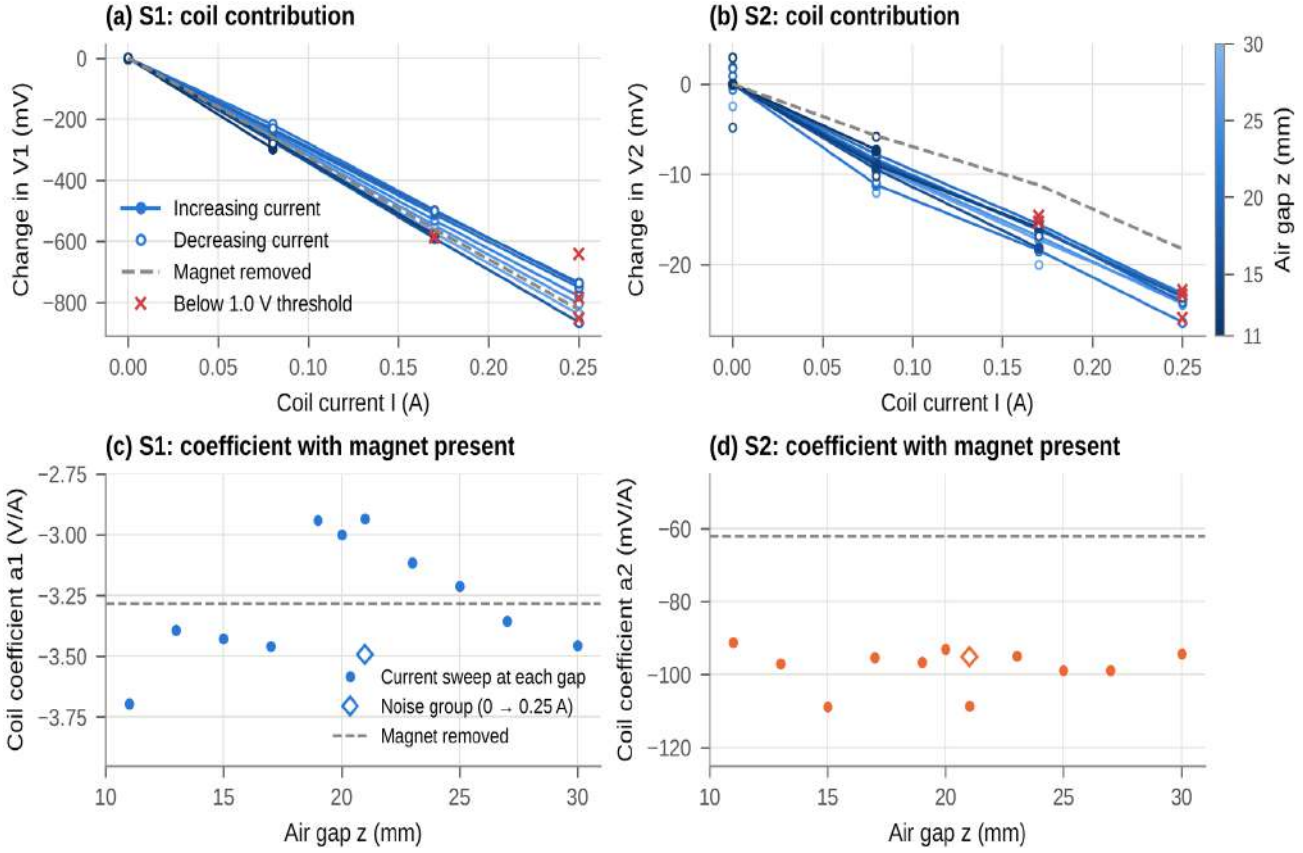


Figure 3: Coil interference: change of (a) S1 and (b) S2 output with coil current at each gap (colour) and with the magnet removed (dashed); filled markers increasing and open markers decreasing current; crosses readings below the 1.0 V threshold. Coil coefficient of (c) S1 and (d) S2 identified at each gap with the magnet present.

Coefficients with the magnet from the increasing branch above 1.0 V. Below about 0.95 V the incremental S1 slope between 0.17 and 0.25 A fell to −2575 mV/A at 13 mm and −688 mV/A at 11 mm (Section IV-D).

C. Lateral Cross-Sensitivity

Fig. 4 shows the measured lateral profiles of S1 at zero current against the scale position. All accepted profiles are asymmetric: a displacement towards positive x weakened the field at S1 (raised V1) much more than one towards negative x. At the operating gap, +2 mm changed the output by 12.1 mV, equivalent to 0.59 mm, and −2 mm by −6.3 mV (0.31 mm); for ±4 mm the equivalent errors were 1.46 and 0.34 mm. For the accepted profiles inside the levitation window (19–25 mm) the smaller of the two ±2 mm errors was 0.31–0.54 mm and the larger 0.59–1.02 mm (median 0.88 mm); the larger ±4 mm error was 1.46–2.02 mm. The profiles at 15 and 17 mm, which failed the consistency check, gave much larger and irregular changes (up to 6.1 mm for +2 mm) and are shown but not interpreted further.

The asymmetry indicates that the magnet axis did not pass through the sensing element at $x = 0$. Fitting the off-axis model with G and δ fixed from the axial calibration and only the axis position and an offset voltage free reproduced the accepted profiles with RMS deviations of 0.5–3.0 mV (at most 0.12 mm in gap) and placed the axis 3.4–6.3 mm on the negative side of $x = 0$. These positions lie at or beyond the edge of the scanned range of ±4 mm, so they are extrapolations that indicate the direction and order of magnitude of the offset rather than measured values; an offset of this size is plausible because the sensors were placed near the face centres without a millimetric reference. Extrapolated to a sensor exactly on the magnet axis, where the profile is flat, the model gives 0.14 mm for ±2 mm at the operating gap; this is a model projection and was not measured.

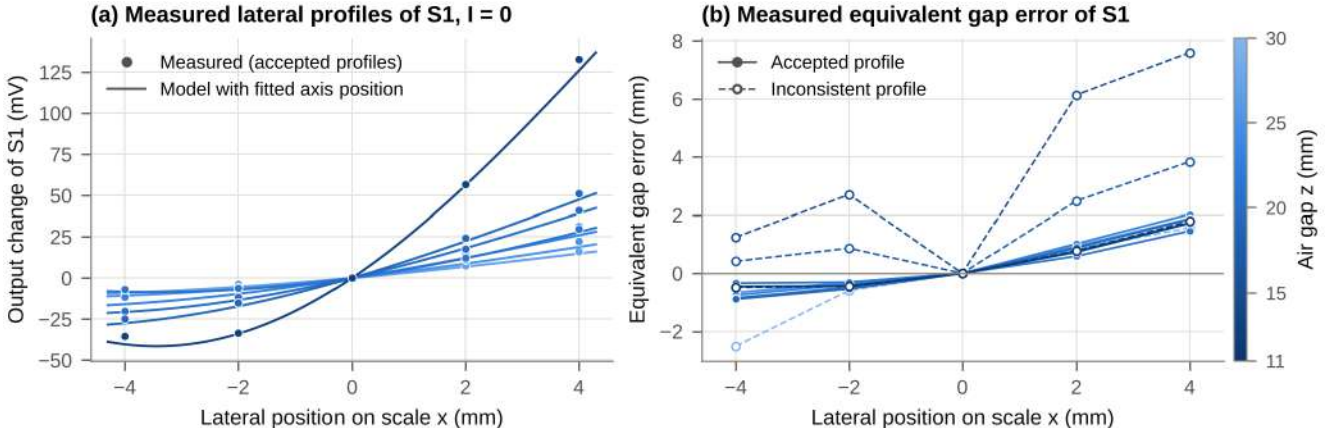


Figure 4: Lateral cross-sensitivity of S1 at $I = 0$ versus the scale position: (a) measured output change for the accepted profiles (markers) and off-axis model with the calibration parameters and a fitted axis position (lines); (b) measured equivalent gap error for all profiles, dashed for the profiles that failed the consistency check. Colour denotes the gap.

D. Readings Below the 1.0 V Threshold

Twelve of the 214 readings were below the 1.0 V threshold, all of them S1 readings between 0.89 and 1.00 V at gaps of 15 mm or less and currents of 0.17 A or more (Fig. 5); S2 stayed between 2.16 and 2.22 V. The highest of them, 998.5 mV, was recorded at 15 mm, $x = 0$ and 0.25 A, just inside the lower edge of the levitation window. The readings themselves show where the response departs from linearity. At 15 mm the incremental slope between 0.17 and 0.25 A (−3338 mV/A) still matched the lower currents, although the final reading was below 1.0 V. At 13 mm, where the output reached 930 mV, it fell to −2575 mV/A, and at 11 mm, between 948 and 893 mV, to −688 mV/A. Compression therefore set in only below about 0.93–0.95 V, consistent with the typical lower end of the SS49E output span [16], so the 1.0 V threshold is slightly conservative. Combining the calibration with the mean coil coefficient gives an estimate of the current at which S1 reaches 1.0 V:

$$I_{\lim}(z) = \frac{V_1(z) - V_{\min}}{|a_1|} \tag{8}$$

At the rated current this estimated boundary lies at 14.4 mm, and at 13.4–15.5 mm for ±1 SD of the coil coefficient; the reading at 15 mm falls within this band. The boundary is therefore an estimate with an uncertainty of about ±1 mm, and since the threshold is a software limit set above the observed onset of compression, it does not mark sensor saturation. Along the holding-current curve from the jump test the estimated S1 output stayed above 1.32 V. At the operating gap the holding current of 0.12 A leaves 0.13 A to the rated current and about 0.20 A to the estimated 1.0 V boundary (0.32 A).

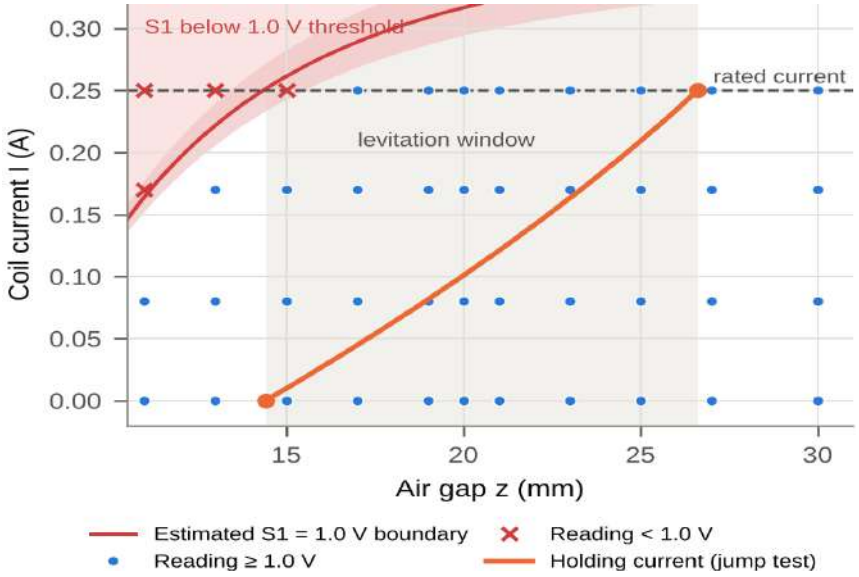


Figure 5: Operating map of S1: estimated current at which S1 reaches the 1.0 V software threshold for the mean coil coefficient (line) and ±1 SD (band), readings above and below the threshold, and holding current from the jump test across the levitation window (shaded).

E. Noise, Drift and Repeatability

In the noise group (Fig. 6) the ten readings at 0 A had standard deviations of 0.56 mV (S1) and 0.60 mV (S2), equivalent to 0.027 and 0.63 mm. The fluctuations of the two sensors were almost identical (correlation 0.98), which points to the shared 5 V supply rather than to the Hall elements, and suggests ratiometric acquisition as a simple improvement. At 0.25 A the S1 output rose steadily by

11.6 mV over ten readings (0.57 mm), whereas S2 rose by 1.5 mV, consistent with the pole face carrying S1 warming under the 2.9 W coil loss; no comparable trend was present at 0 A.

The two repeat sweeps agreed with a pooled standard deviation of 0.11 mm (maximum 0.23 mm), which characterises the resetting of the gap with the caliper. When the zero-current reading of the main sweep is included, the pooled standard deviation of the three readings per gap rises to 0.48 mm, because at 19–27 mm the main-sweep readings lay 8–38 mV above the repeat sweeps. This between-run reproducibility is reported separately from the repeatability.

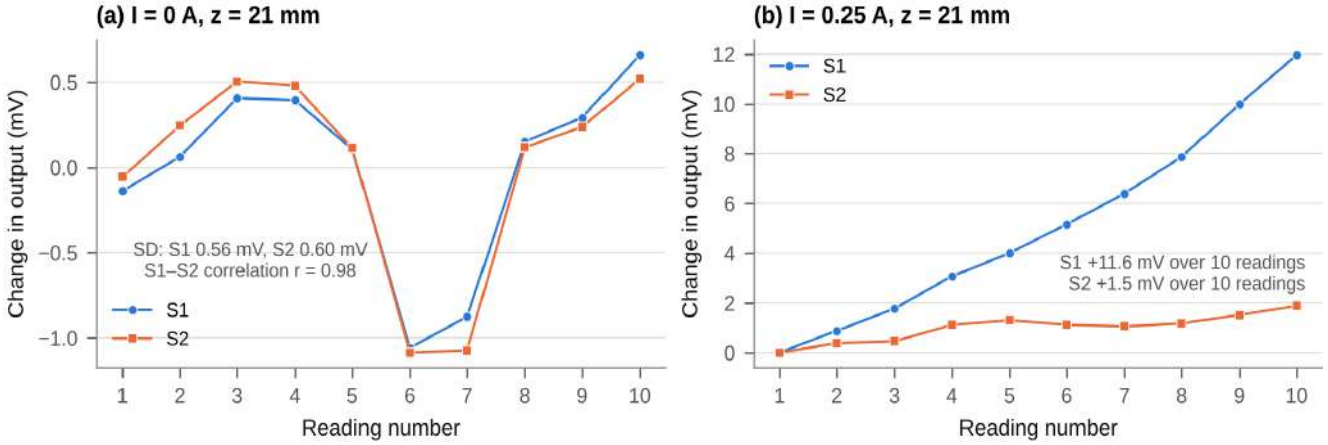


Figure 6: Consecutive readings at the operating gap without moving the rig: (a) deviation from the mean at 0 A; (b) change relative to the first reading at 0.25 A.

F. Comparison of Measurement Architectures

Table 4 and Figure 7 compare the architectures over the levitation window. The static error combines the noise and the current term; the lateral and drift terms are listed separately. Without compensation the coil contribution dominates both sensors: the median static error is 31.5 mm for S1 and 21.1 mm for S2. All compensated variants were evaluated on the decreasing branch of each sweep. With the coefficient identified on the increasing branch of the same sweep (M3, same gap), the equivalent current residual had a median of 0.26 mm (0.14–0.96 mm); the largest value inside the window occurred at 21 mm (19.7 mV, 0.96 mm). A coefficient not identified at the gap in use performed worse on the same readings: the mean coefficient of the other gaps left 1.82 mm (0.55–3.17 mm) and the coil-only coefficient 1.78 mm (0.46–2.99 mm), which reflects the 7.6% scatter of the coefficient between gaps. The sub-millimetre result therefore applies to a coefficient identified near the operating gap and tested within the same sweep. The measured lateral term of S1 for ±2 mm (median 0.88 mm) exceeded the same-gap current residual at every window gap with an accepted profile except 21 mm, so in this installation the sensor alignment, rather than the coil, limited the static accuracy.

The dual-sensor difference M4 performed poorly: 6.1 mm with the same-gap ratio and 9.4 mm with the coil-only ratio. Because the magnet sensitivity ratio $S_1/S_2 \approx 21$ is smaller than the coil ratio $k \approx 27$–41, the difference signal (6) has an inverted sign at every gap and only 25–85% of the S1 sensitivity, whereas the S2 noise, the lateral change of S2 and the reading scatter are multiplied by k. The same amplification raised the measured lateral term to 4.3 mm and the drift to 3.2 mm, against 0.88 and 0.49 mm for S1.

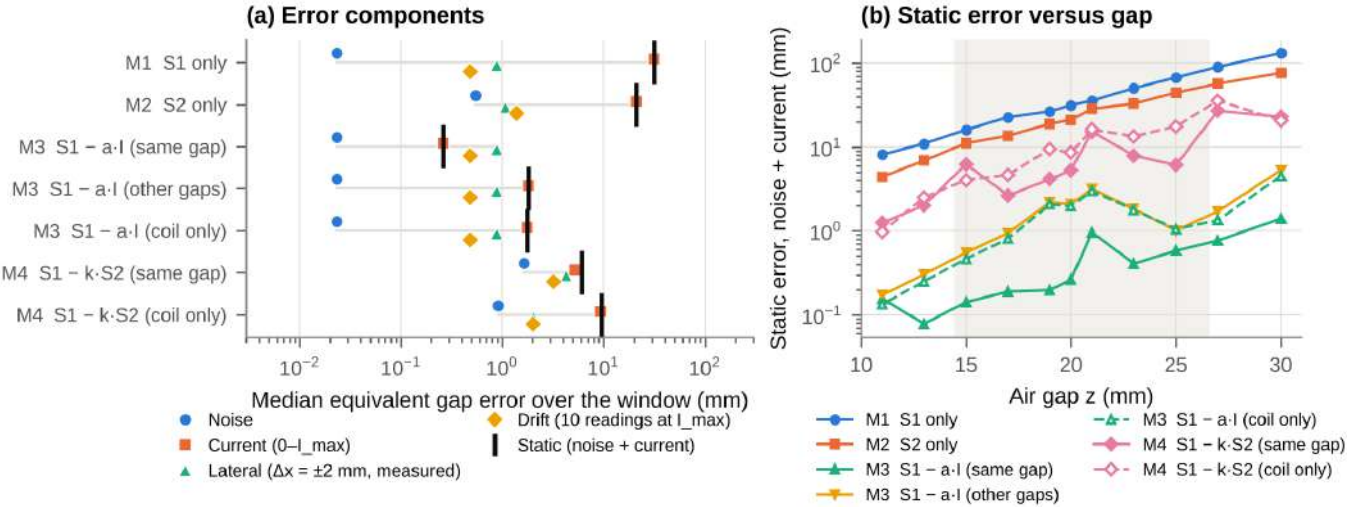


Figure 7: Comparison of measurement architectures: (a) error components, median over the levitation window (15–25 mm), lateral term from the accepted profiles; (b) static error (RSS of noise and current terms) versus gap; levitation window shaded.

Table 4: Equivalent gap error of the architectures, median over the levitation window (mm)

Architecture	Noise	Current	Static	Static range	At 21 mm	Lateral†	Drift*
M1 S1 only	0.023	31.5	31.5	16.0–67.3	35.7	0.88	0.49
M2 S2 only	0.54	21.1	21.1	11.1–44.4	28.5	1.08	1.39
M3 S1 − $a \cdot I$, same gap	0.023	0.26	**0.26**	0.14–0.96	0.96	0.88	0.49
M3 S1 − $a \cdot I$, other gaps	0.023	1.82	1.82	0.55–3.17	3.17	0.88	0.49
M3 S1 − $a \cdot I$, coil only	0.023	1.78	1.78	0.46–2.99	2.99	0.88	0.49
M4 S1 − $k \cdot$S2, same gap	1.64	5.20	6.08	2.64–15.2	15.2	4.26	3.22
M4 S1 − $k \cdot$S2, coil only	0.92	9.41	9.45	4.04–17.5	16.1	2.06	2.01

Static: RSS of the noise and current terms. Current: M1, M2 full coil contribution over 0–0.25 A; M3, M4 largest residual on the decreasing branch of each sweep (common validation readings, not used for the same-gap coefficient).

G. Uncertainty Budget

Table 5 gives an uncertainty estimate for M3 with the same-gap coefficient at the operating gap, obtained with the GUM method [18] under the assumption that the listed components are independent and follow the stated distributions (normal for the Type A terms, rectangular for the Type B maxima). The largest contributions are the compensation residual, the calibration residual (0.46 mm), which includes the between-run reproducibility of the three readings per gap, the measured lateral term and the drift. With the residual of the 21 mm sweep (19.7 mV, the largest inside the window) the expanded uncertainty is 1.73 mm; with the median residual of all gaps (7.1 mV) it is 1.38 mm, and 1.22 mm without the drift term. These values depend on the assumptions above and refer to this installation, with its off-axis sensor.

Table 5: Uncertainty estimate of M3 at z = 21 mm (S_1 = 20.5 mV/mm)

Source	Type	u (mm), A	u (mm), B
Noise, SD of 10 readings	A	0.027	0.027
ADC quantisation, 1 LSB/√12	B	0.003	0.003
Calibration residual	A	0.463	0.463
Compensation residual, max/√3	B	0.553	0.200
Lateral ±2 mm, measured max/√3	B	0.341	0.341
Drift, 10 readings, max/√3	B	0.327	0.327
Combined u_c		0.863	0.692
Expanded U (k = 2)		**1.73**	**1.38**

Column A uses the compensation residual of the 21 mm sweep (validation branch); column B the median residual of all gaps.

V. DISCUSSION

The results answer the placement question for this class of electromagnet. The pole-face location gives the gap information: S1 is 21 times more sensitive than S2, and

†Measured larger change for ±2 mm at I = 0, accepted profiles in the window (19–25 mm). *Drift over ten consecutive readings at 0.25 A. Window gaps: 15, 17, 19, 20, 21, 23 and 25 mm.

readings below the 1.0 V threshold occurred only at or below the lower edge of the window. Its coil contribution can be largely removed by a current term, because it was nearly linear and almost unchanged by the magnet, but only with a coefficient identified close to the operating gap (0.26 mm against about 1.8 mm for a transferred coefficient). Over a wider operating range, a gap-scheduled coefficient or periodic re-identification would therefore be needed.

The location near the back face performed poorly. The dual-sensor scheme of [8] assumes that the coil field is similar at both ends of the electromagnet, whereas the magnet field decays strongly between them. In the measured data the coil coefficient at S2 was about 27–53 times smaller than at S1 (with and without the magnet), whereas the magnet sensitivity was only about 21 times smaller. A plausible explanation is that the closed steel case of the pot-type electromagnet returns most of the coil flux inside the case, so that S2 sees a strongly reduced coil field; the effect of the case on the magnet field was not measured separately, so this interpretation remains to be confirmed, for example with a field simulation. Whatever the cause, the coil-cancelling ratio k exceeded the magnet sensitivity ratio, and the difference signal was inverted, attenuated and loaded with k times the S2 noise. Symmetric multi-sensor layouts on the pole face [6], [7] avoid this problem because all sensors see the coil field through the same geometry.

The lateral results translate into a mounting rule. For the accepted profiles (13 and 19–27 mm) a displacement of ±2 mm changed the S1 reading by the equivalent of 0.3–1.0 mm, more than the compensated current term, and the response was strongly asymmetric. The asymmetry is consistent with a sensing element several millimetres away from the magnet axis at x = 0, which is plausible for a sensor placed by eye. The analytical model suggests that a sensor centred on the axis would see a lateral displacement only as a second-order error (0.14 mm for 2 mm at the operating gap), but this projection was not tested. Because an off-axis sensor produces an asymmetric profile, a lateral scan such as that of Fig. 4 offers a simple check before use: the sensor is centred when the profile becomes symmetric.

The study has limitations. The measurements are static, so dynamic effects such as eddy currents in the steel and the bandwidth of the sensor chain are not covered; only one

magnet and one electromagnet were tested; the two sensors were not exchanged, so differences in their individual gain, offset and orientation are not separated from the effect of their location; the coil current was taken from the supply display rather than measured independently; the axis position was estimated by extrapolation from a ±4 mm scan; the drift at the rated current was observed over a short sequence and calls for temperature compensation or periodic re-identification of the coefficient; and the closed-loop performance of the recommended architecture remains to be verified.

VI. CONCLUSION

For a pot-type maglev electromagnet the gap sensor belongs on the pole face. A sensor there carries the gap information, and its coil interference, although large, is nearly linear and can be removed with a current term, provided that the coefficient is identified near the operating gap. A second sensor near the back face did not help in this rig, because the coil-cancelling ratio exceeded the magnet sensitivity ratio. In this static study the remaining error was dominated by the alignment of the sensor with the magnet axis, so centring the sensor, checked with a lateral scan, matters as much as compensating the coil. Future work will verify the compensated, centred sensor in closed-loop levitation with temperature compensation.

FUNDING

This research received no external funding.

DATA AVAILABILITY

The measurement table and the analysis scripts are available from the corresponding author on reasonable request.

DECLARATION OF AI USE

During the preparation of this work the author used Claude (Anthropic) for language editing and for support in writing the code used to produce the figures. The author reviewed and verified all content and takes full responsibility for the published article.

REFERENCES

[1] S. J. Abu Bakar, K. J-Shenn, P. Goh, and N. S. Ahmad, "Development of magnetic levitation system with position and orientation control," *Int. J. Reconfigurable Embedded Syst.*, vol. 12, no. 2, pp. 287–296, 2023. Available from: https://doi.org/10.11591/ijres.v12.i2.pp287-296

[2] J.-H. Yang, T.-S. Kim, S.-Y. Shim, Y.-S. Lee, and O.-K. Kwon, "Actuator and sensor modeling for magnetic levitation system," in *Proc. Int. Conf. Control, Automation and Systems (ICCAS)*, Seoul, Korea, Oct. 2007. Available from: https://doi.org/10.1109/ICCAS.2007.4407034

[3] T. Bächle, S. Hentzelt, and K. Graichen, "Nonlinear model predictive control of a magnetic levitation system," *Control Eng. Pract.*, vol. 21, no. 9, pp. 1250–1258, 2013. Available from: https://doi.org/10.1016/j.conengprac.2013.04.009

[4] Z. Huang, J. Zhu, J. Shao, Z. Wei, and J. Tang, "Recurrent neural network based high-precision position compensation control of magnetic levitation system," *Sci. Rep.*, vol. 12, Art. no. 11435, 2022. Available from: https://doi.org/10.1038/s41598-022-15638-0

[5] El Hajjaji and M. Ouladsine, "Modeling and nonlinear control of magnetic levitation systems," *IEEE Trans. Ind. Electron.*, vol. 48, no. 4, pp. 831–838, 2001. Available from: https://doi.org/10.1109/41.937416

[6] Z. Zhang and H. Zhang, "Symmetric Hall-effect-based distance sensor for zero-power permanent-electromagnetic suspension (PEMS) system," *IEEE Sens. J.*, vol. 23, pp. 25844–25853, 2023. Available from: https://doi.org/10.1109/JSEN.2023.3314790

[7] Z. Zhang, L. Chen, X. Luo, and S. Yan, "Transformed magnetic force model of zero power permanent electromagnetic suspension system by using Hall effect based distance sensor," *Sci. Rep.*, vol. 15, Art. no. 10952, 2025. Available from: https://doi.org/10.1038/s41598-025-95317-y

[8] Reznichenko and P. Podržaj, "Design methodology for a magnetic levitation system based on a new multi-objective optimization algorithm," *Sensors*, vol. 23, no. 2, Art. no. 979, 2023. Available from: https://doi.org/10.3390/s23020979

[9] L. Castellanos Molina, R. Galluzzi, A. Bonfitto, A. Tonoli, and N. Amati, "Magnetic levitation control based on flux density and current measurement," *Appl. Sci.*, vol. 8, no. 12, Art. no. 2545, 2018. Available from: https://doi.org/10.3390/app8122545

[10] Z. Németh, C. H. See, K. Goh, A. Ghani, S. Keates, and R. A. Abd-Alhameed, "Machine learning-based position detection using Hall-effect sensor arrays on resource-constrained microcontroller," *Sensors*, vol. 25, no. 20, Art. no. 6444, 2025. Available from: https://doi.org/10.3390/s25206444

[11] X. Zhang, M. Mehrtash, and M. B. Khamesee, "Dual-axial motion control of a magnetic levitation system using Hall-effect sensors," *IEEE/ASME Trans. Mechatronics*, vol. 21, no. 2, pp. 1129–1139, 2016. Available from: https://doi.org/10.1109/TMECH.2015.2479404

[12] J. K. Nørgaard and F. Bentsen, "Zero-power control of hybrid magnetic levitation system," M.Sc. thesis, Dept. Energy Technology, Aalborg Univ., Aalborg, Denmark, 2015. Available from: https://projekter.aau.dk/projekter/files/213558827/MCE4_1024_Report.pdf

[13] Z. Zhang, T. Gao, Y. Qin, J. Yang, and F. Zhou, "Numerical study for zero-power maglev system inspired by undergraduate project kits," *IEEE Access*, vol. 8, pp. 90316–90323, 2020. Available from: https://doi.org/10.1109/ACCESS.2020.2994128

[14] N. Derby and S. Olbert, "Cylindrical magnets and ideal solenoids," *Am. J. Phys.*, vol. 78, no. 3, pp. 229–235, 2010. Available from: https://doi.org/10.1119/1.3256157

[15] E. P. Furlani, *Permanent Magnet and Electromechanical Devices*. San Diego, CA, USA: Academic Press, 2001. Available from: https://tinyurl.com/2cx372b6

[16] Honeywell, "SS39ET/SS49E/SS59ET Series linear Hall-effect sensor ICs," datasheet 50000353, Honeywell International Inc. Available from: https://tinyurl.com/yxj8zrfa

[17] Texas Instruments, "ADS111x ultra-small, low-power, I2C-compatible, 860-SPS, 16-bit ADCs," datasheet SBAS444. Available from: https://www.ti.com/lit/ds/symlink/ads1115.pdf

[18] JCGM, "Evaluation of measurement data—Guide to the expression of uncertainty in measurement," JCGM 100:2008, 2008. Available from: https://doi.org/10.59161/JCGM100-2008E

ABOUT THE AUTHOR



Okan Uyar received the B.Sc. degree in electronics and computer education and the M.Sc. degree in electronics and computer systems education from Selçuk University, Konya, Türkiye, in 2007 and 2010, respectively, and the Ph.D. degree in electrical and electronics engineering from the same university in 2019. He received a second B.Sc. degree in electrical and electronics engineering from Necmettin Erbakan University, Konya, in 2021. He joined Selçuk University in 2008 as a Research Assistant and has been an Assistant Professor with the Division of Control Systems, Department of Mechatronics Engineering, Faculty of Technology, since 2020. His research interests include intelligent and model-predictive control, embedded systems, mobile robotics, machine vision, and the application of machine learning to agricultural and biomedical engineering problems.